A Direct-Coupled Detector for Synchrotron X-Radiation Using a Large Format CCD

Eric F. Eikenberry*, Mark W. Tate†, Andrew L. Belmonte†,
John L. Lowrance‡, Donald Bilderback**, and Sol M. Gruner†

*Department of Pathology, UMDNJ-Robert Wood Johnson Medical School, Piscataway, NJ.
†Department of Physics, Princeton University, Princeton NJ.
‡Princeton Scientific Instruments, Monmouth Jct., NJ.
**Cornell High Energy Synchrotron Source and School of Applied Engineering Physics, Cornell University, Ithaca, NY.

Abstract

A novel x-ray area detector based on a large format charge-couple device (CCD) imaging array has been constructed and characterized. It was found to exhibit high signal to noise ratio, wide dynamic range and high spatial resolution. Tests with both conventional and synchrotron sources showed the detector to be highly suitable for x-ray diffraction studies.

INTRODUCTION

Synchrotron radiation sources impose stringent requirements on 2-dimensional (area) x-ray detectors to be used for diffraction studies. Desirable features that should be considered in selecting such a detector include:

- Quantum limited detection for low energy x-rays (*e.g.*, 6 to 30 keV) in order to achieve the highest feasible signal to noise ratio with the wavelengths typically used in diffraction studies;
- High spatial resolution to record patterns made with microbeam collimation and to maximize the number of Bragg reflections that can be resolved in crystals with large unit cells;
- Wide dynamic range so that the full scale of diffracted intensity can be recorded with a single exposure;
- Ability to record at extremely high flux rates for conventional and time-resolved studies. As an example, Laue patterns from protein crystals have been recorded from single 120 ps undulator pulses at the Cornell High Energy Synchrotron Source (CHESS), demonstrating a peak diffracted flux greater than 4×10^{14} x-ray/s [1,2];
- Rapid, on-line data readout to facilitate alignment and exposure verification as well as to collect data;
- Large active area to permit data collection from wide angle scattering;
- Immunity to the intense electrical noise that can be present at synchrotron facilities;
- Small physical size to facilitate incorporation into the beam-line instrumentation.

The high data rates encountered with a synchrotron source require an integrating x-ray detector design[3]. The traditional detector medium is x-ray film, which integrates and has the operational advantages of being easy to use and well understood. But film is very far from quantum limited in its ability to detect low energy x-rays and requires considerable processing to render its data into computer compatible format. Accordingly, numerous investigators have sought to devise improved detectors, the most significant recent advances being in optical based detectors with charge-coupled device (CCD) imaging array readout [3,4,5], and in optically read storage phosphors [6,7,8].

We have designed and constructed a prototype of a new generation of x-ray detectors in which the primary energy converter is directly coupled to a large format CCD without intervening lenses or optical gain. Test results under a variety of conditions show that this detector meets most of the criteria listed above. Directions for future development of this type of detector are briefly discussed.

DETECTOR DESIGN

Figure 1 schematically depicts the relations of the major elements of the detector. Figure 2 shows the carrier of the active components in two states of partial disassembly.

The CCD was a model TEK 2048M (Tektronix, Inc, Beaverton, OR), a 2048 × 2048 pixel imaging array employing 27 μm square pixels [9]. The active area of this

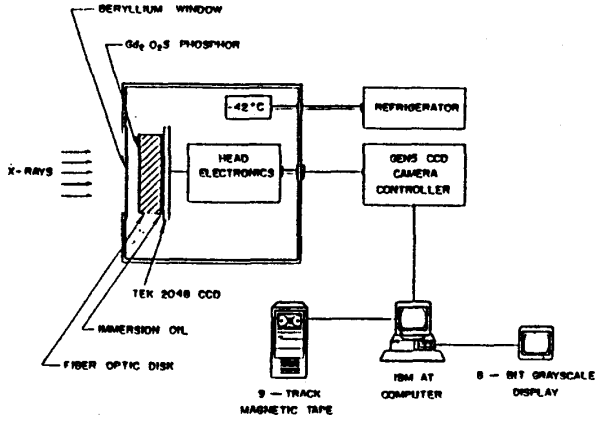

Fig. 1 Schematic diagram of the detector.

0018-9499/91/0400-0110$01.00 © 1991 IEEE

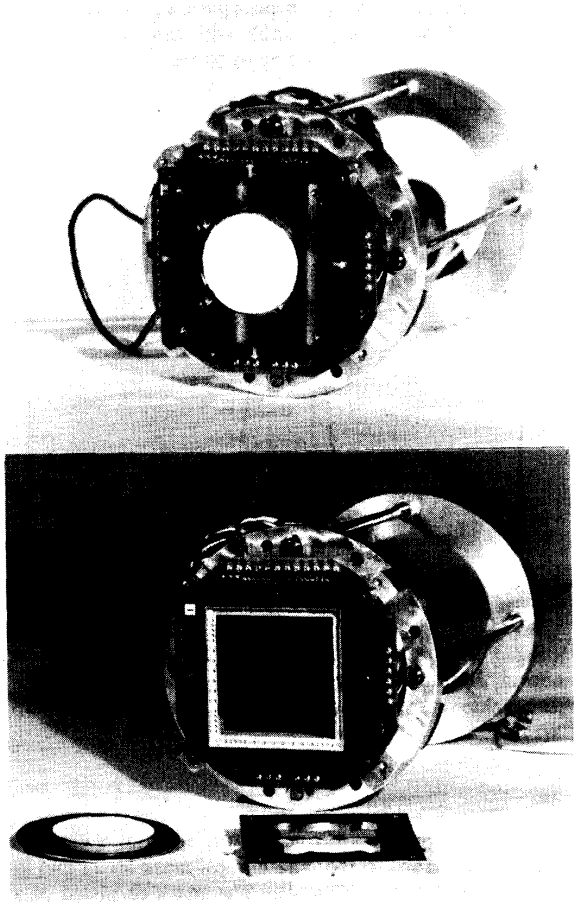

Fig. 2 (Top) Photograph of the CCD carrier with the 50 mm diameter fiber optic disk and phosphor in place. This assembly slides into the cooled copper jacket of the cryostat to position the phosphor 25 mm behind the beryllium window. (Bottom) Photograph of the CCD carrier with the fiber optic disk (lower left) and its brass holder (lower right) removed. The CCD is seen at the center. The silicon die, including the wire bonding pads, measures 85 mm across the diagonal.

CCD is a square 55.3 mm on edge. The device available for these experiments was a grade 3 chip that was basically a developmental prototype with limited availability. The chip had a number of bad columns, visible at the left side of images shown below, and had other blemishes as well. Many of the latter could be removed by background subtraction.

X-rays enter the detector through a 0.005" (125 μm) beryllium window 125 mm in diameter and impinge on the phosphor (primary energy converter) located about 30 mm behind the window. The phosphor, deposited on a fiber optic disk 50 mm diameter and 5 mm thick, was gadolinium oxysulfide (terbium doped) (Nichia Chemical Industries, Tokushima, Japan) coated at a density of 8.4 mg/cm^2 (27 μm) in a cellulose nitrate binder. A brass fixture was fabricated to hold the fiber optic disk lightly against the surface of the CCD. When the fiber optic was mounted, a 50 μl drop of immersion oil (laser liquid, code 1056 R.P. Cargille Laboratories, Cedar Grove, NJ) was placed on the CCD surface to improve optical coupling and to cushion the possibly harsh contact between the glass and the CCD. This polysiloxane oil had a pour point of −70 °C and was tested to have a residual ion content below 1 ppm to protect the CCD surface from chemical degradation. The CCD assembly was placed in a bell jar and evacuated for 10 min to remove air bubbles from the oil.

The CCD, carrying the brass fixture and fiber optic, was installed in a socket supported on a carrier (Fig. 2) that permitted the assembly to be fixed in place behind the beryllium window inside the cryostat (300 mm × 300 mm × 400 mm deep). The cryostat, internally insulated with polyurethane foam, was cooled with the cooling probe of a mechanical refrigeration unit (CryoCool CC-80, Neslab, Inc., Portsmouth, NH) at a rate of 10 °C per hour. The cryostat was additionally insulated on the exterior with polyurethane foam, and provided with a 10 W heater to eliminate condensation on the beryllium window. Most of the experiments reported here were performed with the cryostat cooled to -42 °C (measured at the CCD), which was at the lower limit of the refrigerator's capability. Temperature was controlled by cycling of the refrigerator, which produced slowly varying temperature excursions of *ca.* ±1 °C (measured at the CCD) that complicated quantitative measures of dark current and noise (see discussion).

The CCD was operated by a Princeton Scientific Instruments (Monmouth Jct., NJ) Model V camera which features a slow scan readout (25 μs per pixel) for low noise and a 16 bit analog to digital converter (ADC). The camera was controlled by an IBM PC/AT computer equipped with 10 Mbyte of extended memory, a 9-track 6250 BPI tape drive, and an 8-bit grayscale display. Software for reading the CCD was provided by Princeton Scientific Instruments and data reduction software was written by us.

Detector Characterization

Saturation

The gain of the electronics was set such that 10.4 electrons in the CCD gave one count in the ADC. Optical tests of the CCD with a resolution test pattern prior to installation in the detector demonstrated that saturation of the chip ("full well", corresponding to an incipient loss of modulation in the test pattern) corresponded to approximately 8 × 10^5 electrons, exceeding the range of the ADC. Thus, the ADC limited the maximum signal that could be measured.

Efficiency

The efficiency of the detector system was measured with a calibrated ^{55}Fe source (*ca.* 10 mCi collimated through a 6 mm hole at a distance of 100 mm) that emitted 4.01×10^3 x-ray/cm^2/s measured at the position of the phosphor. It was found that each 5.9 keV x-ray produced 16 electrons (1.5 ADC counts) in the CCD.

Dark Current

The dark charge and the statistical fluctuation in the dark charge were measured for accumulation times ranging from 1 s to 10^4 s. It was found that the dark charge increased linearly with time over the entire range of accumulation times. The dark current was 13 e$^-$/s, corresponding to 0.8 x-ray/s (referred to ^{55}Fe), a figure which could be reduced considerably by further cooling of the CCD. The standard deviation of the dark charge measurements, expressed as electrons, accurately fitted $4.8 \times (\text{time})^{1/2}$ + constant, as would be expected of a Poisson process. This figure would also be reduced by further cooling. The constant, which represents the inherent readout noise of the system, corresponded to 22 electrons, or approximately 1.4 x-ray. Thus the dynamic range of the system for a single exposure, given by the ratio of a full scale reading to the readout out noise, was 3×10^4. The synchrotron exposures reported below (*cf.* Fig. 4) utilized more than half of this dynamic range.

"Zinger" Rate

Highly sensitive quantum limited detectors such as this one show random bright pixels or groups of pixels that accumulate with time. These events, called "zingers", are attributable to cosmic rays and to radioactive decays in the fiber optic blank adjacent to the phosphor. We measured the zinger rate in 3000 s accumulations to be 4×10^{-7}/s/pixel on the phosphor, and 6×10^{-8}/s/pixel in the corners of the CCD not covered by the fiber optic disk. The latter rate, about one event every four seconds over the entire CCD, is consistent with a cosmic ray origin. For quantitative measurements of x-ray doses, as reported here, both exposures and backgrounds are made in pairs and zingers are removed in software before further analysis.

Uniformity

A portable x-ray generator with Ni filtered Cu radiation was used set up at a distance of 1.73 m from the detector to provide uniform x-ray illumination. Figure 3 shows a histogram of the values of 10^6 pixels from a centrally located square on the detector image. The mean value was 11,500 x-ray/pixel. The histogram is a smooth distribution with a FWHM (full width at half-maximum) of 8% of the mean value. This nonuniformity arises from pixel to pixel variations in the sensitivity of the phosphor and of the CCD. These spatial variations are stable with time, allowing the nonuniformity to be corrected by software.

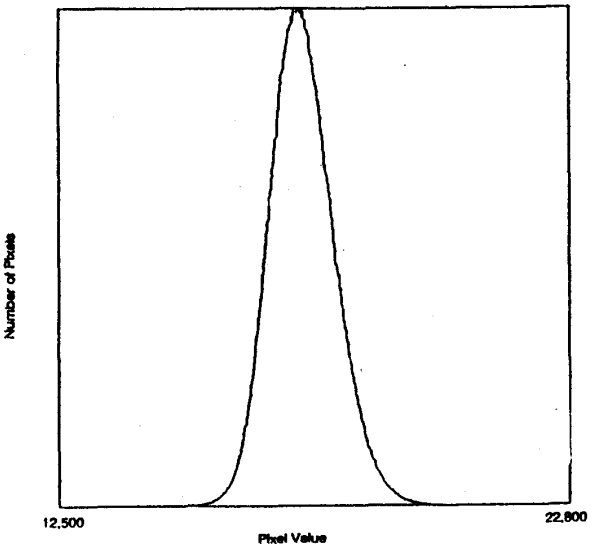

Fig. 3 Histogram of the values of 10^6 pixels exposed to uniform illumination by Ni filtered Cu radiation. The mean value corresponds to 11,500 x-ray/pixel, and the FWHM is 8% of the mean.

Resolution

The portable x-ray generator, again at a distance of 1.73 m, was used to illuminate a test mask set 31 mm in front of the phosphor (Fig. 4). The mask consisted of a square grid of 75 μm diameter lithographically formed holes on 1 mm centers in a sheet of 0.005" (125 μm) tungsten (Towne Laboratories, Sommerville, NJ). Images of 137 holes from the center of the pattern were averaged together and then cylindrically averaged to form an average spot profile. This was deconvoluted for hole profile and for the profile of the source target to obtain a best fit Gaussian point spread function (PSF). The calculated PSF had a FWHM of 1.8 pixel, or 50 μm. The narrowness of this PSF is demonstrated directly in the scan shown below (*cf.* Fig. 7).

Distortion

The mask image used to determine the PSF was also analyzed for distortion. The centroids of the 137 hole images described above were all within 0.35 pixel (9.5 μm) of an ideal square grid fitted to the pattern. Thus, distortion was unmeasurably low, as would be expected from the construction of the detector if there were no appreciable shear in the fiber optic disk.

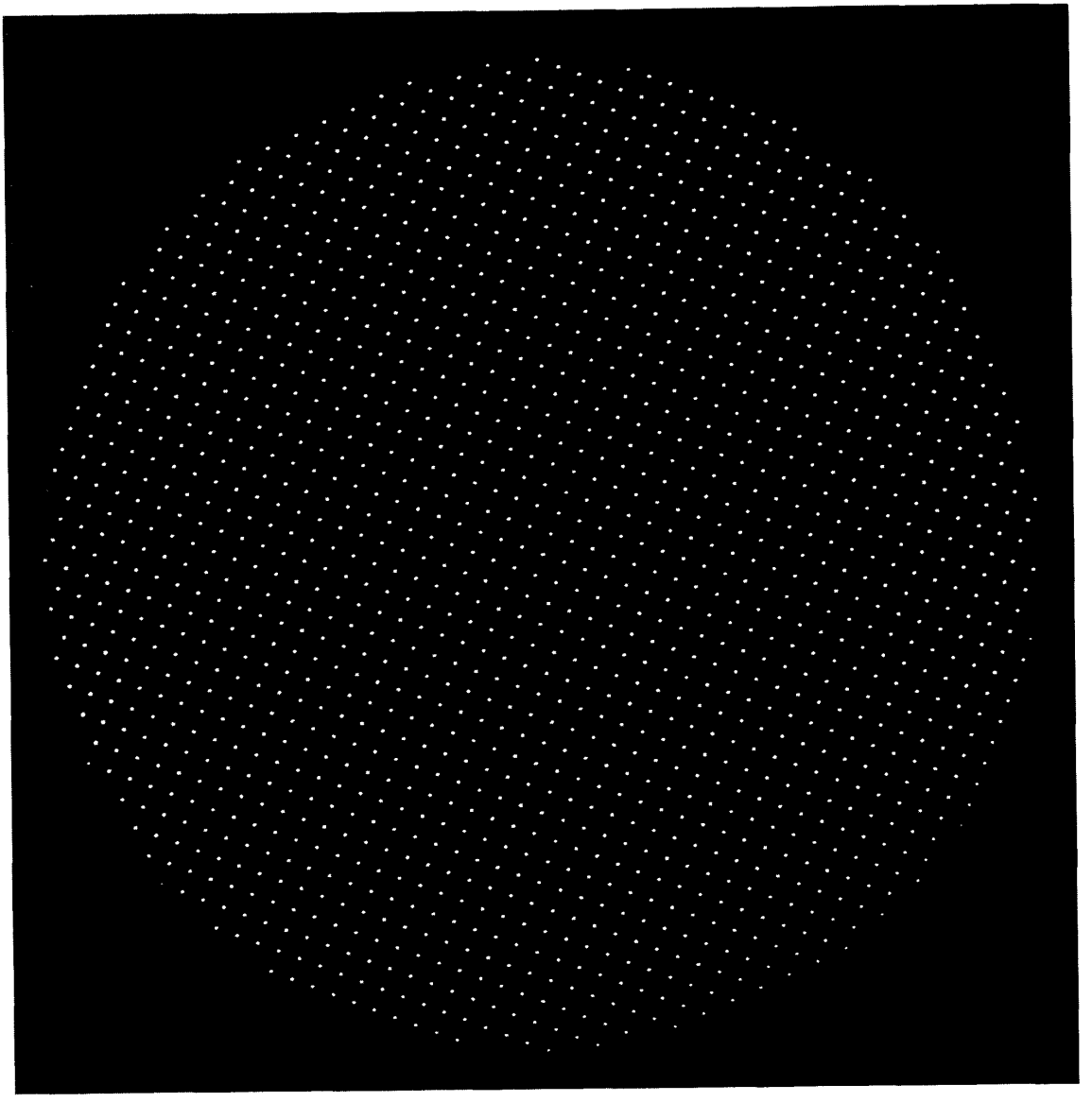

Figure 4 X-ray image of the test mask. The holes in the tungsten sheet are 75 μm in diameter and lie on 1 mm centers.

Detective Quantum Efficiency (DQE)

We were unable to determine the DQE directly [10,11] because the ^{55}Fe source was capable of delivering only one x-ray per pixel every 30 s, while the dark current, due to insufficient cooling, was about 20 times larger. This is not as disadvantageous for a detector as it might at first seem: in a 1000 s exposure, the standard deviation in the signal due to x-ray statistics would roughly equal the standard deviation due to dark current, *ca.* 120 e$^-$/pixel. But, it does make the extraction of a DQE figure very dependent on the model assumed for the analysis. However, the high efficiency of the detector for low energy x-rays together with the absence of deviations from linear behavior, indicate that the DQE is limited primarily by the quantum efficiency of the phosphor. The DQE in that case is given by:

$$\begin{aligned} \text{DQE} &= (\text{signal/noise})^2_{\text{out}} / (\text{signal/noise})^2_{\text{in}} \\ &\approx \epsilon/(1 + 1/g) \end{aligned}$$

where ϵ is the numerical quantum efficiency of the phosphor, g is the visible photon yield per x-ray (assumed to be a Poisson process), and the subscripts out and in refer to the detector output and the x-ray input respectively. ϵ can be identified with the attenuation by the phosphor since essentially all x-rays that are stopped emit light. Although g will increase with energy, it has little effect on the statis-

Fig. 5 Laue diffraction pattern of a gallium arsenide/gallium aluminum arsenide multilayered crystal recorded with an x-ray beam collimated to 20 μm diameter. The exposure time was 1 s, and the beam intensity was estimated to be 10^{11} x-ray/s. The inset shows a 32× enlargement of the reflections on either side of the arrow.

tics of the detector output, and hence on the DQE, because it is already a large number at low energy. However, the value of g will affect measured intensities at different energies. Table I gives the calculated attenuation and relative luminous gain (ϵg) of the gadolinium oxysulfide used here at various x-ray energies.

Tests with a conventional source

X-ray diffraction patterns of several phospholipid liquid crystal and collagen fiber specimens were recorded with the detector on the rotating anode beam-line at Princeton. This line is equipped with double mirror optics and provides *ca.* 2×10^7 x-ray/s (8.0 keV) in a focal spot of 0.2 × 2 mm. Patterns of excellent quality were obtained in 15 to 45 min which, in terms of signal to noise and ability to record weak reflections, were comparable to the patterns obtained

Table I
Calculated Attenuation and Relative Luminous Gain for the Gd_2O_2S Phosphor

Energy, keV	Calculated Attenuation	Relative Luminous Gain
6	85%	0.59
8	97%	0.90
10	86%	1.0
20	27%	0.63
30	10%	0.35

with the intensified detector systems that have been reported from this laboratory [12].

Tests at CHESS

Laue x-ray micro-diffraction patterns were recorded at the B2 beam-line at CHESS. Figure 5 is a 1 s exposure from a gallium arsenide/gallium aluminum arsenide evaporated multilayered crystal showing superlattice reflections from the layered structure. The sample, a square thin plate 40 μm on edge, was affixed to the end of a leaded glass capillary, 2 cm in length with an inside diameter of 20 μm, which served as the collimator. The intensity of the 20 μm diameter continuous spectrum beam was *ca.* 10^{11} x-ray/s. The inset shows a 32× enlargement of two of the diffraction peaks. The complex shape of the reflections is caused by internal reflections in the collimator and mosaic spread in the crystal. Figure 6 shows a scan 1 pixel wide along the set

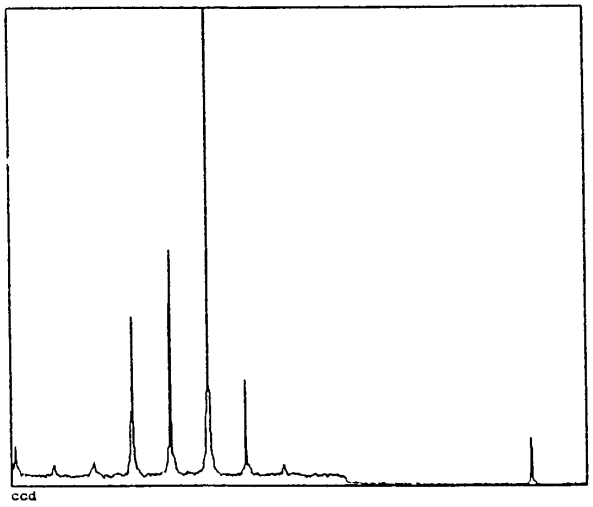

Fig. 6 A scan 1 pixel in width along the line of reflections indicated by the arrow in Fig. 5. The high signal to noise ratio and excellent spatial resolution are apparent.

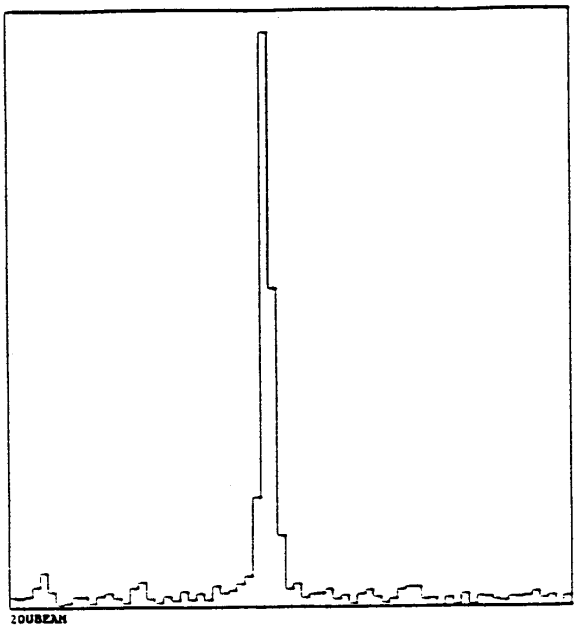

Fig. 7 Enlargement of the scan through the central beam shown at the right in Fig. 6. Each step represents 1 pixel = 27 μm on the phosphor.

of reflections shown enlarged in the inset of Fig. 5, and extending through the central beam which penetrates the beamstop. The excellent signal to noise characteristics of the detector are manifest. Figure 7 shows an enlargement of the scan through the central beam, directly illustrating the narrow PSF (note that the beam itself is almost 1 pixel in diameter).

Figure 8 shows a 2 s Laue microdiffraction pattern of crystalline lysozyme, again using a 20 μm diameter leaded glass capillary as the collimator. The tetragonal crystal (space group $P4_32_12$) was mounted in a sealed capillary and measured *ca.* 150 μm in the direction of the beam. The complex appearance of some of the reflections is again due to mosaic spread in the crystal and internal reflections in the collimator. The brightest reflection has at least 7 separate components that can be seen in the original image in addition to the halo; these components are not seen in images with detectors having lower spatial resolution.

Efficiency vs. Energy

The diffraction pattern of lysozyme shown in Fig. 8 was simultaneously recorded on a storage phosphor plate. The pattern was analyzed to index the reflections, identify their energy and integrate their intensity. Thirty-five matching reflections were also integrated in the detector image and the ratios were averaged to measure the detector's efficiency relative to that of the storage phosphor as a function of wavelength. Dividing the ratios by the known efficiency

Fig. 8 Laue diffraction pattern of tetragonal lysozyme recorded with an x-ray beam collimated to 20 μm diameter. The exposure time was 2 s, and the beam intensity was estimated to be 10^{11} x-ray/s.

of the storage phosphor [7,13] and normalizing gave the relative efficiency of the detector shown in Table II. It is seen that the efficiency of the CCD-based detector appeared to drop somewhat from 15 to 30 keV, but not as much as would be expected from the reduction in the stopping power of the phosphor over this range. The unexpectedly high apparent efficiency can be attributed in part to x-rays which penetrate the fiber optic blank and directly excite the CCD. Based on the density and mass absorption coefficient of silicon, this mechanism could produce *ca.* 25% of the total observed signal at 30 keV. Possible luminescence within the fiber optic could also contribute to the signal. It should be noted that these figures are uncertain because of the difficulty in estimating the background near the reflections because of their complex shape.

Summary

Table III summarizes the operating characteristics of the CCD detector.

Table II
Relative Efficiency of CCD Detector vs. Energy

Energy Range, keV	Relative Efficiency
11.5 - 13.6	1.0 ± 0.2
14.2 - 17.4	1.2 ± 0.2
27 - 33	0.8 ± 0.2

Table III
Summary of the CCD Detector Parameters

CCD	TEK 2K, 2048 × 2048 pixels
Pixel Size	27 μm × 27 μm
Phosphor	Gd_2O_2S, 8.4 mg/cm², 50 mm dia.
PSF	<50 μm, FWHM
Sensitivity	16 e^-/x-ray, ^{55}Fe
Saturation	4×10^4 x-ray/pixel
Dynamic Range	3×10^4
Dark Current	13 e^-/pixel/s @ -42 °C
	(0.8 x-ray/pixel/s)
Dark Current Noise	4.8 e^-/pixel/$s^{-1/2}$ @ -42 °C
	(0.3 x-ray/pixel/$s^{-1/2}$)
Readout Noise‡	22 e^- (1.4 x-ray)
Linearity	Excellent
Distortion	< 0.35 pixel
"Zinger" Rate†	4×10^{-7}/pix/s on phosphor
	6×10^{-8}/pix/s off phosphor
Readout Time*	110 s

‡Includes some dark current because of the readout time
†See text
*See discussion

Discussion

We have constructed and tested a direct coupled 2-dimensional x-ray detector utilizing a large format CCD as the image readout device. It features wide dynamic range, quantum limited sensitivity and high resolution, and operates as an integrating detector that is well suited to diffraction studies with synchrotron radiation. The prototype detector has been thermally cycled more than six times and transported to and from CHESS with no apparent degradation in performance.

It is worth noting that the wide dynamic range reported here applies to a single image. The exposure reproduced in Figure 5 utilizes more than half of the reported dynamic range (*ca.* 40% of full well) with no evidence of blooming or image degradation in the original image. Since there are no optical elements to degrade the image with scattered light, the dynamic range can in principle be increased further by summing multiple images; however, this would require software and storage to accommodate more than 16 bits per pixel.

Selecting an optimum phosphor for Laue diffraction studies is difficult. Gadolinium oxysulfide was chosen here because of the wide energy range that was anticipated at the synchrotron, even though our measurements show yttrium oxysulfide (Tb) to be more efficient at 8 keV and below. Experiments showed there to be a broad maximum in the efficiency of a phosphor as a function of increasing thickness; therefore, we selected a thickness near the low end of this maximum in order to optimize resolution. This phosphor did not have good attenuation for higher energy x-rays, thereby limiting the performance of the detector in this realm. However, to obtain attenuation to 1/e for 30 keV x-rays would require more than 250 μm of Gd_2O_2S which, as a uniform layer, would severely compromise the resolution. It may be noted that intagliated phosphors have the potential to achieve high stopping power while maintaining good resolution [14,15].

Future improvements of this design can be suggested in several areas. It would be desirable to further reduce the dark current and noise by lowering the CCD temperature, and control the temperature more precisely to facilitate quantitative measurements. A reduction of temperature by 10 °C can be expected to reduce the dark current 5-fold. In addition, precautions need to be taken to minimize the thermal gradient across the CCD, which produced noticeable variations in dark current from the center to the edge in the experiments reported here. It would also be helpful to package the detector in a smaller housing to facilitate mounting on the beam-line. Use of a thicker special low radioactivity fiber optic disk for the phosphor would reduce the zinger rate in the active area of the detector and prevent x-rays from reaching the CCD. A faster readout of the chip, possibly using four quadrant readout, would be helpful in increasing the experimental throughput. This would have the additional benefit of reducing the readout noise. Finally, interposing a fiber optic reducing taper between the phosphor and the CCD could be used to greatly increase the useable area of the detector at the sacrifice of some of the resolution. Tapers up to 110 mm diameter are currently available. For example, the use of a 1.5:1 taper would reduce the sensitivity to 10 e^-/x-ray and increase the PSF to 70 μm while increasing the sensitive area to 80 mm × 80 mm. The losses introduced by a taper will reduce the DQE at the lowest integrated doses for low energy x-rays.

ACKNOWLEDGEMENTS

The authors thank T.-Y. Teng for providing lysozyme crystals, Alan LeGrand for reading the storage phosphors and sharing his storage phosphor efficiency data, Marian Szebenyi for interpreting the lysozyme pattern and Bernie Weinstein for providing the multilayered crystal. We also thank Erramilli Shyamsunder, Peter So and Joe Strzalka for generously helping to gather the data at CHESS, Martin Novak for constructing parts of the detector, and Philip Karcher for help in making prints of images. This work was supported by DOE (contract DE-FG02-87ER60522) and NIH (grant GM32614 and SBIR grant R43RR04384.01A1).

REFERENCES

[1] D.M.E. Szebenyi, D.H. Bilderback, A. LeGrand, K. Moffat, W. Schildkamp, and T.-Y. Teng, "120 Picosecond Laue Diffraction Using an Undulator X-ray Source", *Trans. Am. Crystal. Assoc.*, vol. 24, pp. 167-172, 1988.

[2] D.M.E. Szebenyi, D.H. Bilderback, A. LeGrand, K. Moffat, W. Schildkamp, B. Smith Temple and T.-Y. Teng, "Laue Diffraction Patterns Recorded with a 120 Picosecond Exposure from an X-ray Undulator", submitted for publication.

[3] S.M. Gruner "CCD and vidicon x-ray detectors: Theory and practice", *Rev. Sci. Instr.*, vol. 60, pp. 1545-1551, 1989.

[4] R.H. Templer, S.M. Gruner, and E.F. Eikenberry, "An Intensified CCD Area X-ray Detector for use with Synchrotron Radiation", in *Advances in Electronics and Electron Physics*, vol. 74, pp. 275-283, 1988.

[5] M.G. Strauss, I. Naday, I.S. Sherman, M.R. Kraimer, E.M. Westbrook, and N.J. Zaluzec, "CCD Sensors in Synchrotron X-ray Detectors", *Nucl. Instr. Meth.*, vol. A266, 563-577, 1988.

[6] B.R. Whiting, J.F. Owen, and B.H. Rubin, "Storage Phosphor X-ray Diffraction Detectors", *Nucl. Instr. Meth.*, vol. A266, pp. 628-635, 1988.

[7] D. Bilderback, K. Moffat, J. Owen, B. Rubin, W. Schildkamp, D. Szebenyi, B. Smith Temple, K. Volz, and B. Whiting, "Protein Crystallographic Data Acquisition and Preliminary Analysis Using Kodak Storage Phosphor Plates", *Nucl. Instr. Meth.*, vol. A266, pp. 636-644, 1988.

[8] Y. Amemiya, T. Matsushita, A. Nakagawa, Y. Satow, J. Miyahara, and J. Chikawa, "Design and Performance of an Imaging Plate System for X-ray Diffraction Study", *Nucl. Instr. Meth.*, vol. A266, pp. 645-653, 1988.

[9] M.M. Blouke, B. Corrie, D.L. Heidtmann, F.H. Yang, M. Wizenread, M.L. Lust, H.H. Marsh IV, and J.R. Janesick, "Large Format, High Resolution Image Sensors", *Opt. Engineering*, vol. 26, pp. 837-843, 1987.

[10] S.M. Gruner, J.R. Milch, and G.T. Reynolds, "Evaluation of Area Photon Detectors by a Method Based on Detective Quantum Efficiency", *IEEE Trans. Nucl. Sci*, vol. NS-25, pp. 562-565, 1978.

[11] S.M. Gruner, and J.R. Milch, "Critera for the Evaluation of 2-Dimensional X-ray Detecors", *Trans. Am. Crystal. Assoc.*, vol. 18, pp. 149-167, 1982.

[12] S.M. Gruner, J.R. Milch, and G.T. Reynolds, "Slow-scan silicon-intensified target-TV x-ray detector for quantitative recording of weak x-ray images", *Rev. Sci. Instrum.*, vol 53, pp. 1770-1778, 1982.

[13] A.D. LeGrand, personal communication.

[14] K. Oba, M. Ito, M. Yamaguchi, and M. Tanaka, "A CsI(Na) Scintillation Plate with High Spatial Resolution", in *Advances in Electronics and Electron Physics*, vol. 74, pp. 247-255, 1988.

[15] V. Duchenois, M. Fouassier, and C. Piaget, "High Resolution Luminescent Screens for Image Intensifier Tubes", in *Advances in Electronics and Electron Physics*, vol. 64B, pp. 365-371, 1985.